Preprint Title Synthesis and potent cytotoxic activity of diosgenin derivative FZU-0021-194-P2 and its phytosomes against non-small-cell lung cancer cells

Authors Liang Xu, Dekang Xu, Ziying Li, Yu Gao and Haijun Chen

Article Type Full Research Paper

ORCID® iDs Yu Gao - https://orcid.org/0000-0002-1137-7669

Synthesis and potent cytotoxic activity of diosgenin derivative FZU-0021-194-P2 and its phytosomes against non-small-cell lung cancer cells

Liang Xu[1,2#], Dekang Xu[1,2#], Ziying Li[1,2], Yu Gao[1,2*], and Haijun Chen[1,2**]

1 Cancer Metastasis Alert and Prevention Center, and Pharmaceutical Photocatalysis of State Key Laboratory of Photocatalysis on Energy and Environment, College of Chemistry, Fuzhou University, Fuzhou, Fujian 350116, China.

2 Fujian Provincial Key Laboratory of Cancer Metastasis Chemoprevention and Chemotherapy, Fuzhou University, Fuzhou, Fujian 350116, China.

#L. Xu and D. Xu contributed equally to this work.

Corresponding authors:

* Yu Gao, PhD, College of Chemistry, Fuzhou University, Fuzhou, Fujian 350108, China. Email: hellogaoyu@126.com

** Haijun Chen, PhD, College of Chemistry, Fuzhou University, Fuzhou, Fujian 350108, China. Email: chenhaij@gmail.com

Abstract

Diosgenin (Di), a steroidal sapogenin derived from plants, has been shown to exert anti-cancer effects in preclinical studies. Using Di as a starting material, various Di derivatives were designed and synthesized, aiming to discover new steroid-based antitumor agents. In this work, we synthesized several Di derivatives and screened FZU-0021-194-P2 (P2), which showed more potent cytotoxic activities against human non-small-cell lung cancer A549 and PC9 cells. Considering that Di has a unique sterol structure similarly to cholesterol, P2 phytosomes (P2P) were prepared to further improve the water solubility of P2. P2P exhibited a particle size of 53.6 ± 0.3 nm with oval shape and a zeta potential of −4.0 ± 0.7 mV. P2P could inhibit the proliferation of lung cancer cells more efficiently than Di phytosomes with 72-h incubation time through the mechanism of inducing cell cycle arrest and apoptosis. The results indicated that P2P could be a promising anticancer formulation for non-small-cell lung cancer.

Keywords

Diosgenin; Non-small-cell lung cancer; Sterol structure; Phytosomes

1 Introduction

Natural products are the most feasible source of leading compounds in exploitation of anti-cancer drugs [1]. In recent years, chemists have shown great passion for seeking effective new chemical entities (NCE) from natural products and their derivatives. Diosgenin (3β-hydroxy-5-spirostene, Di), is a conventional herbal sterols distilled from yams, fenugreek, and Costus speciosus [2]. Prominently, it is a characteristic initial intermediate for the synthesis of steroidal compositions, oral contraceptives and sex hormones. A series of preclinical and mechanistic investigations showed that Di contributed to multiple anti-cancer activities, such as restraining the hTERT gene expression in A549 lung cancer cells [3], inhibiting breast cancer stem-like cells by the Wnt β-catenin signaling [4], impeding hepatocellular carcinoma cells by increasing DDX3 expression [5], and inducing prostate cancer cell apoptosis through activation of estrogen receptor-β [6]. Additionally, studies in recent decades demonstrated that Di has unique preventive/therapeutic outcomes not only against tumors, but also for other diseases such as diabetes [7], myocardial infarction (AMI) [8], acute liver injury [9], goiter [10], and alzheimer's disease (AD) [11].

In consideration of the diverse biological activities of Di, researchers are interested in modifying the steroid structure of Di to obtain Di derivatives which had more efficient anti-cancer activities than that of Di. 1-Phenyl-(1H-1,2,3-triazol-4yl)-methoxy diosgenin, which is a simple phenyl R moiety attached via triazole to the parent molecule, showed almost three times decrease in IC_{50} value against A549 cells than that of Di [12]. Diosgenin–imidazolium salt derivatives were also synthesized and displayed significant cytotoxic activities against several human cancer cell lines

[13]. One of novel 22-oxo-26-selenocyanocholestanic steroids based on Di synthesized by Herrera *et al.* exhibited remarkable antiproliferative activity against Hela cells which is close to the clinical anticancer agent paclitaxel [14]. These successful examples demonstrated the promising steroidal structure of Di for discovery of new anticancer drugs.

Liposomes which were usually constituted of phospholipids and stabilized by cholesterol have been substantially investigated as drug carriers for targeting, modulating drug pharmacokinetics, and decreasing drug toxicity [15, 16]. Liposomes also can be used as solubilizing media to enhance solubility and bioavailability of insoluble drugs [17]. Di and our prepared analogues have an extremely similar sterol structure to cholesterol. It was reported that Di and the lipids formed highly stable complexes at the air/water interface [18]. Therefore, Di and its derivatives could be substituted for cholesterol to form novel stable liposome-like phytosomes. The prepared phytosomes were expected to enhance the solubility and bioavailability of the Di derivative for clinical transformation.

In this study, we first prepared several Di derivatives and screen the most potent candidate through the preliminary structure–activity relationship study. Then the liposome-like phytosomes were prepared by substituting Di and its derivative for cholesterol. The anti-cancer effects of free drugs and their phytosomes were investigated in non-small cell lung cancer cells.

2 Results and discussion

2.1 Synthesis and characterization of Di derivatives

Late stage functionalization (LSF), which uses the C-H bonds as points of potential variation, is a useful method to generate novel analogs of a lead structure without

depending on *de novo* synthesis [19]. Recently, it is widely accepted that the aliphatic C-H oxidation could be an efficient approach to diversify complex structures at the sites remoting from the existing functionalities [20]. In the steroid structure of Di, there are abundant electrons in the double bond site for electrophilic addition. Based on this feature, we designed and synthesized a series of Di derivatives. The novel Di derivative FZU-0021-194-P2 (P2) which showed the most efficient effects of suppressing cell growth was screened (**Figure 1**). The structure of P2 was further established by X-ray crystallographic analysis. CCDC1844665 contains the crystallographic data of P2. The data can be obtained free of charge from the Cambridge Crystallographic Data Center.

2.2 Anti-proliferative activity of P2

The anti-cancer effects of Di and its analogue P2 were tested in human lung cancer A549 and PC9 cell lines, human cervical cancer Hela cell line, and human hepatoma HepG2 cell line using MTT assays. All cells were treated with each compound at indicated concentrations for 48 h. It was found that Di and P2 could suppress two lung cancer cells more sensitively than Hela and HepG2 cells (**Table 1**). The IC_{50} values of P2 in A549 and PC9 cells were 11.8 and 15.2 μM, respectively, which were much lower than those of Di (55.0 and 85.8 μM, respectively). **Figure 2A** shows that Di and P2 could suppress the cell viability in a dosage dependent manner in A549 and PC9 cells. All the results demonstrated that P2 had much stronger antiproliferative activity against A549 and PC9 cells than that of Di.

2.3 Cell cycle arrest and apoptosis induced by P2

Cell cycle is the series of events that take place in cells for their propagation and multiplication. The phases consist of the Gap 1 phase (G1), Synthesis phase (S),

Mitosis phase (M), and Gap 2 phase (G2). Di induced cell cycle arrest in different phases against different cancer cells. It was reported that Di could induce G2/M cell cycle arrest in liver cancer cells [21], arrest SCC cells at the sub-G1 phase [22], and impede cell cycle progression in the G0/G1 phase in A549 cells [23]. To determine the anti-proliferative mechanisms of Di and P2, the effects of Di and P2 on cell cycle distributions were examined in A549 and PC9 cells. As shown in **Figure 2B**, Di and P2 could induce A549 and PC9 cell cycle arrest in G0/G1 phase (at a concentration 20 μM for A549 cells and 30 μM for PC9 cells for 48 h). To our surprise, the cell proportion in G0/G1 phase induced by P2 at a low concentration (5 μM) was exceeding that of Di at high concentrations. These results demonstrated that P2 was more potent than Di to inhibit cell cycle progression.

Apoptosis, the programmed cell death, is a physiological process that is accurately regulated at genetic level resulting in the removal of damaged cells in a controlled manner [24]. Most of the chemotherapeutic drugs exert effects through the mechanism of apoptosis. It was reported that diosgenin could induce early apoptosis in human prostate DU145 cancer cells [25] and cause late apoptosis in human cervical HeLa cancer cells [26]. In order to explore the death mechanism of P2, A549 and PC9 cells were treated with P2 and Di for 48 h and the proportion of cells undergone apoptosis was counted through Annexin V-FITC/PI staining and followed by flow cytometry analysis. As shown in **Figure 2C**, each scatter plot is divided into four quadrants. The cells in Q1, Q2, Q3, and Q4 quadrants represent necrotic cells, late apoptotic cells, early apoptotic cells, and viable cells, respectively. The results showed that P2 significantly induced apoptosis in both A549 and PC9 cells compared with Di. In A549 cells, P2 at 20 μM induced 51.1% early apoptosis, while Di at the same concentration induced only 3.75% early apoptosis. P2 at 5 μM showed even

stronger early apoptosis induction effects than that of Di at 20 μM. In PC9 cells, P2 at 30 μM induced 34.4% early and late apoptosis, while Di only induced 6.7% early and late apoptosis. The results clearly showed that P2 was more potent than Di in inducing apoptosis in A549 and PC9 cells.

2.4 Preparation and characterization of P2 phytosomes (P2P)

Formulating small-molecule drugs into nanometer-scaled particles have been widely investigated for targeted drug delivery to tumors. These nanoparticles can passively accumulate in tumors via enhanced permeability and retention (EPR) effect, thus decreasing the toxicity of non-selective bio-distribution [27]. Considering the advantages of liposomes as a drug delivery system for chemotherapeutic drugs and the similar sterol structures in cholesterol and Di, complexes of phospholipids and Di or P2 were prepared to further enhance the solubility and improve the pharmacokinetic profiles of Di and P2 for better clinical transformation.

Phytosomes are lipid compatible molecular complexes of phospholipids and natural active ingredients, in which the active ingredients containing sufficient polar functional groups such as COOH, OH, NH_2 are anchored to the polar head of phospholipids by the polar and hydrogen-bond interactions [28]. Because of the interaction, phospholipids and natural active ingredients could undergo self-assembly into stable structures of vesicles in aqueous solution, which could act as a vehicle to facilitate membrane transport [29]. Compared to liposomes, phytosomes could load more drug molecules, and showed enhanced stability in the lyophilization and reconstitution processes prior to use [30]. Phytosomes have been used as drug delivery systems of several insoluble natural drugs in recent years. Sinigrin [31] and epigallocatechin-3-O-gallate [32] loaded in phytosomes showed stronger

antiproliferative activities than free drugs against melanoma cells and breast cancer cells, respectively.

In this work, Di phytosomes (DiP) and P2 phytosomes (P2P) were prepared by a thin-film rehydration method (**Figure 3A**). Blank lipid nanoparticles (P) were also prepared with the same process without drug. The particle sizes and zeta potentials of phytosomes were detected by dynamic light scattering (DLS). The characteristics of phytosomes were summarized in **Table 2**. P2P showed the minimum size with an average diameter of about 53.6 ± 0.3 nm and DiP showed the slightly larger size with an average diameter of about 66.3 ± 0.3 nm (**Figure 3B**). Nevertheless, P showed the maximum size with an average diameter of about 139.8 ± 1.1 nm, almost twice the size of DiP and P2P. The results showed that the addition of Di and P2 could decrease the particle size of lipid nanoparticles. The particle size of 100 nm diameter or less will be more beneficial to the blood circulation and tumor accumulation [33]. Numerous studies have shown that cholesterol is crucial for structural stability of liposomal membranes [34]. The existence of cholesterol analogs Di and P2 in phytosomes could improve the structural stability of phytosomes. The zeta potentials of DiP and P2P were −6.4 and −4.0 mV, respectively. Because the negatively charged particles have weak interactions with negatively charged cell membrane, the anion nanoparticles could have less cytotoxicity than the cationic ones [35]. In addition, it was reported that the anion nanoparticles could be inclined to interact with the lung surfactant to make it more easily accessible into lung cells [36]. Therefore the phytosomes we prepared with size less than 100 nm and negative charges, will be more beneficial to lung cancer treatment.

The morphologies of the DiP and P2P were observed by transmission electron microscopy (TEM) and atomic force microscopy (AFM) (**Figure 3C and 3D**). P2P

and DiP demonstrated roughly homogeneous oval shape under TEM observation but showed spherical morphologies in the figures of AFM. According to the literature, a phytosome will display a micellar shape in aqueous solution [37]. The oval shape of P2P and DiP could be due to the aggregation of phytosomes during the sample preparation for TEM.

2.5 Anti-proliferative activity of P2P

To determine the cytotoxicity of DiP and P2P in lung cancer cells, cells were treated with different concentrations of P, DiP and P2P for different incubation times. The toxicity of the blank lipid nanoparticles was first investigated. As shown in **Figure 4,** P did not show any anti-proliferative effects on A549 and PC9 cells, indicating the safety of the carrier materials. DiP and P2P showed efficient anti-proliferative activity in a dose- and time-dependent manner. DiP and P2P showed no obvious cytotoxicity after 24 h incubation. However, the anti-proliferative effects were greatly improved when the incubation time was extended to 72 h. The results indicated that the entrapped Di and P2 could be sustainedly released from phytosomes to exert effects. As the drugs delivered to the lungs will be quickly eliminated due to large alveolar surface area, abundant capillaries and minimal transport distance, the sustained drug release delivery systems will improve the drug absorption and increase the activities [38]. Compared with DiP, P2P still showed better anti-proliferative effects against A549 and PC9 cells. As comparison, the IC_{50} values of Di and P2 against A549 and PC9 cells after 72 h were also calculated (**Table 1**). The IC_{50} values of Di and P2 against A549 and PC9 at 72 h were lower than the IC_{50} values at 48 h. Compared with free drugs, DiP and P2P showed comparable or better anti-proliferative effects after a 72 h-incubation. The results indicated that phytosomes could be an ideal drug delivery

system for Di and its derivatives to gain sustained-release behavior without affecting drug activity.

2.6 *In vitro* anti-cancer mechanisms of P2P

Cell cycle and cell apoptosis were also investigated in A549 and PC9 cells to study the anti-cancer mechanisms of drug-loaded phytosomes. With 72 h incubation time, DiP and P2P induced cell cycle arrest in G0/G1 phase in A549 and PC9 cells (**Figure 5A**), indicating that the actions of DiP and P2P on cell cycle regulation were the same as those of the free drugs. Compared with DiP, P2P arrested more cells in G0/G1 phase. The results were consistent with the anti-proliferation studies. After 72 h incubation, P2P induced obvious cell apoptosis in A549 and PC9 cells (**Figure 5B**). The cell apoptosis induced by P2P was significantly higher than that induced by DiP, indicating that P2 loaded in phytosomes could retain its anti-cancer activities. As shown in **Figure 2C**, A549 cells treated with P2 after 48 h were almost in the early phase of apoptosis. However, A549 cells treated with P2P after 72 h were almost in the late phase of apoptosis, suggesting that the actions of P2 on induction of cell apoptosis could be altered after loading in phytosomes. One reason might be the changed drug uptake pathway. The free drugs were uptaken by passive transport, while the phytosomes were uptaken through endocytosis [39]. Besides, the phytosomes containing abundant phospholipids could carry amphiphilic agents to cross the cell-membrane barrier to result in high intracellular drug concentration, which might change the action mechanisms of P2.

3 Conclusions

In conclusion, Di derivatives were designed and P2 was screened. P2 showed enhanced *in vitro* cytotoxic activities than that of Di against human non-small-cell

lung cancer A549 and PC9 cells. To further improve the water solubility of Di and P2, DiP and P2P were prepared with a thin-film rehydration method. DiP and P2P exhibited particle sizes less than 100 nm with oval shape and negative charges. Compared with free drugs, DiP and P2P showed comparable or better anti-proliferative effects after a 72 h-incubation, and P2P still showed better anti-proliferative effects through inducing apoptosis and cell cycle arrest against lung cancer cells compared with DiP. All the results indicated that P2P could be a promising anticancer formulation for lung cancer.

4 Experimental section

4.1 Materials

3-(4,5-dimethylthiazol-2-yl)-2,5-diphenyltetrazolium bromide (MTT), DNA-free RNaseA, and propidium iodide (PI) were purchased from Sigma-Aldrich (St Louis, USA). Di was obtained from Energy Chemical (Shanghai, China). RPMI 1640 medium and trypsin-EDTA were purchased from Gibco-BRL (Burlington, ON, Canada). Fetal bovine serum (FBS) was obtained from Gemini (Calabasas, USA). Lecithin and cholesterol were obtained from Sinopharm Chemical Reagent Co., Ltd. (China). All commercially available starting materials and solvents were reagent grade and used without further purification.

Preparative column chromatography was performed using silica gel 60 with particle size 0.063-0.200 mm (70-230 mesh, Flash). Analytical thin layer chromatography (TLC) was carried out employing silica gel 60 F254 plates (Merck, Darmstadt). Nuclear magnetic resonance (NMR) spectra were recorded on a Bruker 400 (^{1}H, 400 MHz; ^{13}C, 101 MHz) spectrometer. Chemical shifts were expressed in

ppm, and J values were given in Hz. High resolution mass spectra (HRMS) were obtained from Thermo Fisher Scientific Exactive Plus mass spectrometer.

4.2 Synthesis and characterization of FZU-0021-194-P2

To a solution of Di (829 mg, 2 mmol) in EtOH (25 mL) was added FePc (28 mg, 0.05 mmol), $NaBH_4$ (378 mg, 10 mmol) and KCNO (811 mg, 10 mmol). The reaction mixture was stirred at r.t. under air for 48 h. The solvent was then evaporated to dryness and the residue was diluted with EtOAc (20 mL) and extracted with H_2O (20 mL). The combined organic layers were washed with saturated brine, dried over anhydrous Na_2SO_4, filtered, which was purified by silica gel chromatography (PE/EtOAc = 4:1) to give the desired product (348 mg, 38%) as a white solid. TLC: R_f = 0.54 (PE/EtOAc = 2:1). ^{1}H NMR (400 MHz, $CDCl_3$) δ 4.38 (d, *J* = 6.3 Hz, 1H), 4.07 – 3.94 (m, 1H), 3.45 (d, *J* = 10.0 Hz, 1H), 3.34 (t, *J* = 11.2 Hz, 1H), 2.04 – 1.94 (m, 2H), 1.87 – 1.80 (m, 2H), 1.76 (d, *J* = 9.9 Hz, 2H), 1.69 (d, *J* = 12.3 Hz, 2H), 1.66 – 1.50 (m, 7H), 1.50 – 1.37 (m, 6H), 1.28 – 1.12 (m, 6H), 1.01 – 0.90 (m, 6H), 0.79 – 0.69 (m, 6H). ^{13}C NMR (101 MHz, $CDCl_3$) δ 121.12, 109.32, 80.83, 67.66, 67.16, 66.92, 62.20, 55.84, 47.13, 43.67, 41.71, 40.72, 39.90, 39.39, 35.06, 34.38, 31.72, 31.70, 31.47, 30.54, 30.35, 28.89, 26.82, 21.30, 17.21, 16.61, 15.42, 14.56. HRMS (ESI): calcd for $C_{28}H_{43}NO_4$ $[M + H]^+$ m/z 458.3265, found 458.3280.

4.3 Preparation of phytosomes

DiP and P2P were prepared with lecithin in the prescribed ratio (1:1, molar ratio) by the thin film hydration method. First, lecithin and Di/P2 were dissolved in chloroform at a molar ratio of 1:1. The organic solvent was evaporated using a rotary evaporator to produce a thin lipid film. Before hydration, the lipid film was dried in a vacuum drying chamber at 27 °C for 12 h. The hydrated multilamellar vesicles were sonicated

by a sonicator for 20 min. Blank lipid nanoparticles (P) were also prepared with the same process without adding Di or P2.

4.4 Characterization of phytosomes

The hydrodynamic diameters and zeta potentials of phytosomes were analyzed by DLS on a Malvern Instruments Zetasizer HS III (Malvern, UK) at room temperature. The morphologies of the phytosomes were detected by atomic force microscopy (AFM, Multimode 8, Bruker, USA) and transmission electron microscopy (TEM, HT7700, Hitachi, Japan).

4.5 Cell cultures

The A549 and PC9 cells were obtained from the Cell Resource Center of Shanghai Institute for Biological Sciences (Chinese Academy of Sciences, Shanghai, China). The A549 and PC9 cells were grown in normal RPMI medium containing 10% FBS. The cells were maintained in a moist cell incubator at 37 °C with 5% CO_2.

4.6 *In vitro* cell viability

Cell viability was determined by MTT assay. Cells seeded in 96-well plates at 70–80% confluence were exposed to free drugs (Di, P2) and phytosomes (P, DiP, P2P) at various concentrations for 48 and 72 h. At the end of the treatment period, viability was determined by the MTT assay [40].

4.7 Cell cycle analysis

A549 and PC9 cells were plated in six-well plates at 2×10^5 cells/well, respectively. The day after plating, the cells were treated with Di or P2 for 48 h and DiP or P2P for 72 h. Then cells were trypsinized and washed with PBS. The cells were fixed with 75% pre-cooled ethanol and kept at 4 °C overnight. Fixed cells were washed with

PBS and incubated with fluorescent solution (1% (v/v) Triton X-100, 0.05% PI, 0.01% RNase A) in dark for 30 min at room temperature. Finally the cells were analyzed by FACS Calibur system and the data was processed and analyzed using the ModFit software (Verity Software House, Topsham, ME) [41].

4.8 Cell apoptosis

For analysis of apoptosis, A549 and PC-9 cells were cultivated with Di or P2 for 48 h and DiP or P2P for 72 h under normoxic condition. Then, cells were harvested, washed with PBS, and collected by centrifugation. The cell suspensions were mixed with 5 μL of FITC-Annexin V, 5 μL of PI, and 500 μL of binding buffer and kept for 15 min in the dark. Subsequently, the apoptotic stages were quantitatively determined by flow cytometry [42].

4.9 Statistical analysis

All data shown in this article were expressed as the mean ± SD for at least three separate experiments. Statistical analysis was performed using the Student's *t*-test.

Acknowledgements

This work received support from the National Natural Science Foundation of China (81871481 and 81571802), the Ministry of Science and Technology of China (2015CB931804), the Natural Science Foundation of Fujian Province (2016J06020), and the Fujian Provincial Youth Top-notch Talent Support Program.

References

1. Li, X., et al., *What makes species productive of anti-cancer drugs? Clues from drugs' species origin, druglikeness, target and pathway.*

Anti-Cancer Agents in Medicinal Chemistry (Formerly Current Medicinal Chemistry-Anti-Cancer Agents), 2019. **19**(2): p. 194-203.
2. Chen, Y., et al., *Advances in the pharmacological activities and mechanisms of diosgenin.* Chin J Nat Med, 2015. **13**(8): p. 578-87.
3. Rahmati-Yamchi, M., et al., *Fenugreek extract diosgenin and pure diosgenin inhibit the hTERT gene expression in A549 lung cancer cell line.* Mol Biol Rep, 2014. **41**(9): p. 6247-52.
4. Bhuvanalakshmi, G., et al., *Breast Cancer Stem-Like Cells Are Inhibited by Diosgenin, a Steroidal Saponin, by the Attenuation of the Wnt beta-Catenin Signaling via the Wnt Antagonist Secreted Frizzled Related Protein-4.* Front Pharmacol, 2017. **8**: p. 124.
5. Yu, H., et al., *Diosgenin increased DDX3 expression in hepatocellular carcinoma.* Am J Transl Res, 2018. **10**(11): p. 3590-3599.
6. Tao, X., et al., *Dioscin induces prostate cancer cell apoptosis through activation of estrogen receptor-beta.* Cell Death Dis, 2017. **8**(8): p. e2989.
7. Khosravi, Z., et al., *Diosgenin ameliorates testicular damage in streptozotocin-diabetic rats through attenuation of apoptosis, oxidative stress, and inflammation.* Int Immunopharmacol, 2019. **70**: p. 37-46.
8. Feng, J., et al., *Biotransformation of Dioscorea nipponica by Rat Intestinal Microflora and Cardioprotective Effects of Diosgenin.* Oxidative medicine and cellular longevity, 2017. **2017**: p. 4176518-4176518.
9. Zheng, L., et al., *Protective effect of dioscin against thioacetamide-induced acute liver injury via FXR/AMPK signaling pathway in vivo.* Biomed Pharmacother, 2018. **97**: p. 481-488.
10. Cai, H., et al., *Diosgenin relieves goiter via the inhibition of thyrocyte proliferation in a mouse model of Graves' disease.* Acta Pharmacol Sin, 2014. **35**(1): p. 65-73.
11. Chojnacki, J.E., et al., *Bivalent ligands incorporating curcumin and diosgenin as multifunctional compounds against Alzheimer's disease.* Bioorg Med Chem, 2015. **23**(22): p. 7324-31.
12. Masood Ur, R., et al., *Synthesis and biological evaluation of novel 3-O-tethered triazoles of diosgenin as potent antiproliferative agents.* Steroids, 2017. **118**: p. 1-8.
13. Deng, G., et al., *Synthesis and antitumor activity of novel steroidal imidazolium salt derivatives.* Eur J Med Chem, 2019. **168**: p. 232-252.
14. Fernandez-Herrera, M.A., et al., *Probing the selective antitumor activity of 22-oxo-26-selenocyanocholestane derivatives.* Eur J Med Chem, 2014. **74**: p. 451-60.
15. Li, F., et al., *Aptamer-Conjugated Chitosan-Anchored Liposomal Complexes for Targeted Delivery of Erlotinib to EGFR-Mutated Lung Cancer Cells.* Aaps j, 2017. **19**(3): p. 814-826.
16. Li, F., et al., *Co-delivery of oxygen and erlotinib by aptamer-modified liposomal complexes to reverse hypoxia-induced drug resistance in lung cancer.* Biomaterials, 2017. **145**: p. 56-71.
17. Mohammed, A.R., et al., *Liposome formulation of poorly water soluble drugs: optimisation of drug loading and ESEM analysis of stability.* Int J Pharm, 2004. **285**(1-2): p. 23-34.

18. Janicka, K., I. Jastrzebska, and A.D. Petelska, *The Equilibria of Diosgenin-Phosphatidylcholine and Diosgenin-Cholesterol in Monolayers at the Air/Water Interface.* J Membr Biol, 2016. **249**(4): p. 585-90.
19. Cernak, T., et al., *The medicinal chemist's toolbox for late stage functionalization of drug-like molecules.* Chem Soc Rev, 2016. **45**(3): p. 546-76.
20. White, M.C. and J. Zhao, *Aliphatic C–H oxidations for late-stage functionalization.* Journal of the American Chemical Society, 2018. **140**(43): p. 13988-14009.
21. Chen, Z., et al., *Diosgenin inhibited the expression of TAZ in hepatocellular carcinoma.* Biochem Biophys Res Commun, 2018. **503**(3): p. 1181-1185.
22. Das, S., et al., *Antineoplastic and apoptotic potential of traditional medicines thymoquinone and diosgenin in squamous cell carcinoma.* PLoS One, 2012. **7**(10): p. e46641.
23. Hsieh, M.J., et al., *Dioscin-induced autophagy mitigates cell apoptosis through modulation of PI3K/Akt and ERK and JNK signaling pathways in human lung cancer cell lines.* Arch Toxicol, 2013. **87**(11): p. 1927-1937.
24. Pistritto, G., et al., *Apoptosis as anticancer mechanism: function and dysfunction of its modulators and targeted therapeutic strategies.* Aging (Albany NY), 2016. **8**(4): p. 603-19.
25. Nie, C., et al., *Diosgenininduced autophagy and apoptosis in a human prostate cancer cell line.* Mol Med Rep, 2016. **14**(5): p. 4349-4359.
26. Zhao, X., et al., *Dioscin induces apoptosis in human cervical carcinoma HeLa and SiHa cells through ROS-mediated DNA damage and the mitochondrial signaling pathway.* Molecules, 2016. **21**(6): p. 730.
27. Yue, X. and Z. Dai, *Liposomal Nanotechnology for Cancer Theranostics.* Curr Med Chem, 2018. **25**(12): p. 1397-1408.
28. Abdelkader, H., et al., *Phytosome-hyaluronic acid systems for ocular delivery of L-carnosine.* Int J Nanomedicine, 2016. **11**: p. 2815-27.
29. Hou, Z., et al., *Phytosomes loaded with mitomycin C-soybean phosphatidylcholine complex developed for drug delivery.* Mol Pharm, 2013. **10**(1): p. 90-101.
30. Shakeri, A. and A. Sahebkar, *Opinion Paper: Phytosome: A Fatty Solution for Efficient Formulation of Phytopharmaceuticals.* Recent Pat Drug Deliv Formul, 2016. **10**(1): p. 7-10.
31. Mazumder, A., et al., *In vitro wound healing and cytotoxic effects of sinigrin-phytosome complex.* Int J Pharm, 2016. **498**(1-2): p. 283-93.
32. Lazzeroni, M., et al., *A Presurgical Study of Lecithin Formulation of Green Tea Extract in Women with Early Breast Cancer.* Cancer Prev Res (Phila), 2017. **10**(6): p. 363-370.
33. Nagayasu, A., K. Uchiyama, and H. Kiwada, *The size of liposomes: a factor which affects their targeting efficiency to tumors and therapeutic activity of liposomal antitumor drugs.* Adv Drug Deliv Rev, 1999. **40**(1-2): p. 75-87.
34. Huang, Z., M.R. Jaafari, and F.C. Szoka, Jr., *Disterolphospholipids: nonexchangeable lipids and their application to liposomal drug delivery.* Angew Chem Int Ed Engl, 2009. **48**(23): p. 4146-9.

35. Shao, X.R., et al., *Independent effect of polymeric nanoparticle zeta potential/surface charge, on their cytotoxicity and affinity to cells.* Cell Prolif, 2015. **48**(4): p. 465-74.
36. Arick, D.Q., et al., *Effects of nanoparticles on the mechanical functioning of the lung.* Adv Colloid Interface Sci, 2015. **225**: p. 218-28.
37. Semalty, A., et al., *Supramolecular phospholipids-polyphenolics interactions: the PHYTOSOME strategy to improve the bioavailability of phytochemicals.* Fitoterapia, 2010. **81**(5): p. 306-14.
38. Loira-Pastoriza, C., J. Todoroff, and R. Vanbever, *Delivery strategies for sustained drug release in the lungs.* Adv Drug Deliv Rev, 2014. **75**: p. 81-91.
39. Babazadeh, A., M. Zeinali, and H. Hamishehkar, *Nano-Phytosome: A Developing Platform for Herbal Anti-Cancer Agents in Cancer Therapy.* Curr Drug Targets, 2018. **19**(2): p. 170-180.
40. Lv, T., et al., *Role of generation on folic acid-modified poly(amidoamine) dendrimers for targeted delivery of baicalin to cancer cells.* Mater Sci Eng C Mater Biol Appl, 2017. **75**: p. 182-190.
41. Zhang, Y., et al., *Folate and heptamethine cyanine modified chitosan-based nanotheranostics for tumor targeted near-infrared fluorescence imaging and photodynamic therapy.* Biomacromolecules, 2017. **18**(7): p. 2146-2160.
42. Zhang, H., et al., *Chitosan-based nanoparticles for improved anticancer efficacy and bioavailability of mifepristone.* Beilstein J Nanotechnol, 2016. **7**: p. 1861-1870.

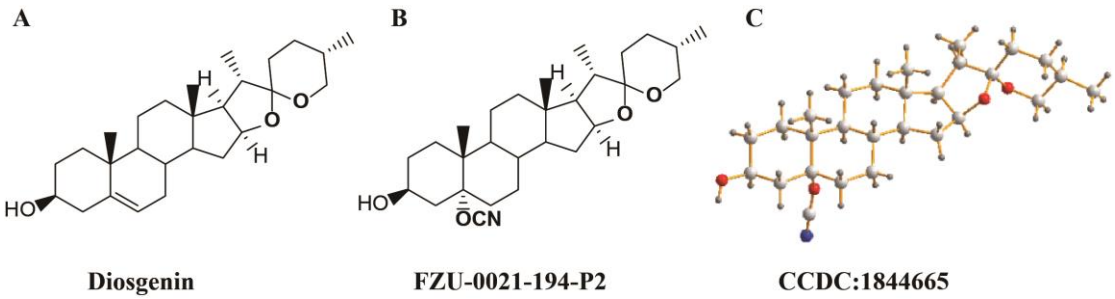

Figure 1 (A) The structure of diosgenin. (B) The structure of FZU-0021-194-P2. (C) X-ray crystallographic analysis of FZU-0021-194-P2. CCDC1844665 contains the crystallographic data of P2. The data can be obtained free of charge from the Cambridge Crystallographic Data Center.

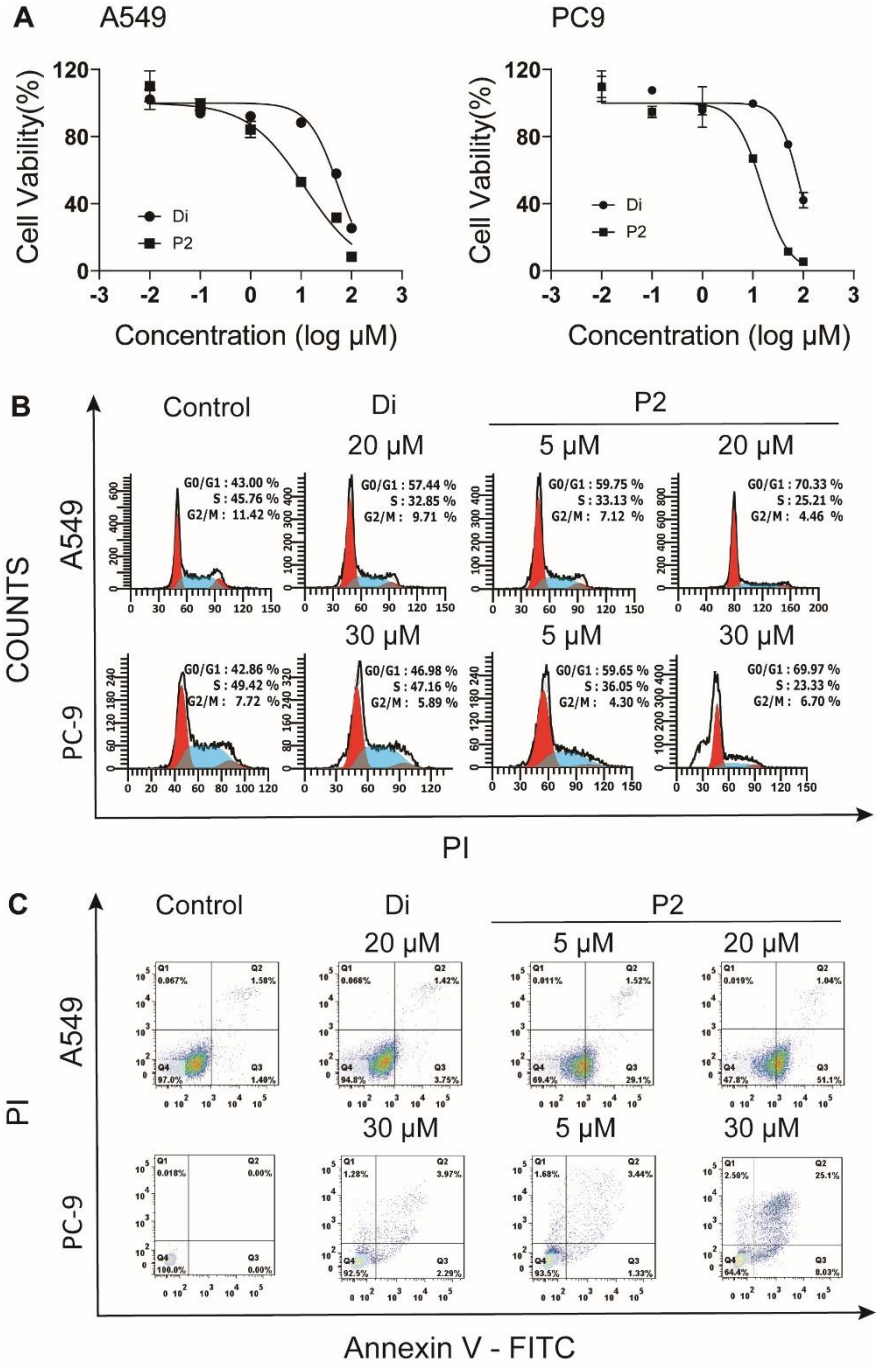

Figure 2 The *in vitro* anti-cancer activities of diosgenin (Di) and its derivative FZU-0021-194-P2 (P2). (A) The anti-proliferative activities of different concentrations of Di and P2 against A549 and PC9 cells for 48 h. (B) Cell cycle analysis of A549 and PC9 cells after treated with Di and P2 for 48 h. (C) Cell apoptosis analysis of A549 and PC9 cells after treated with Di and P2 for 48 h.

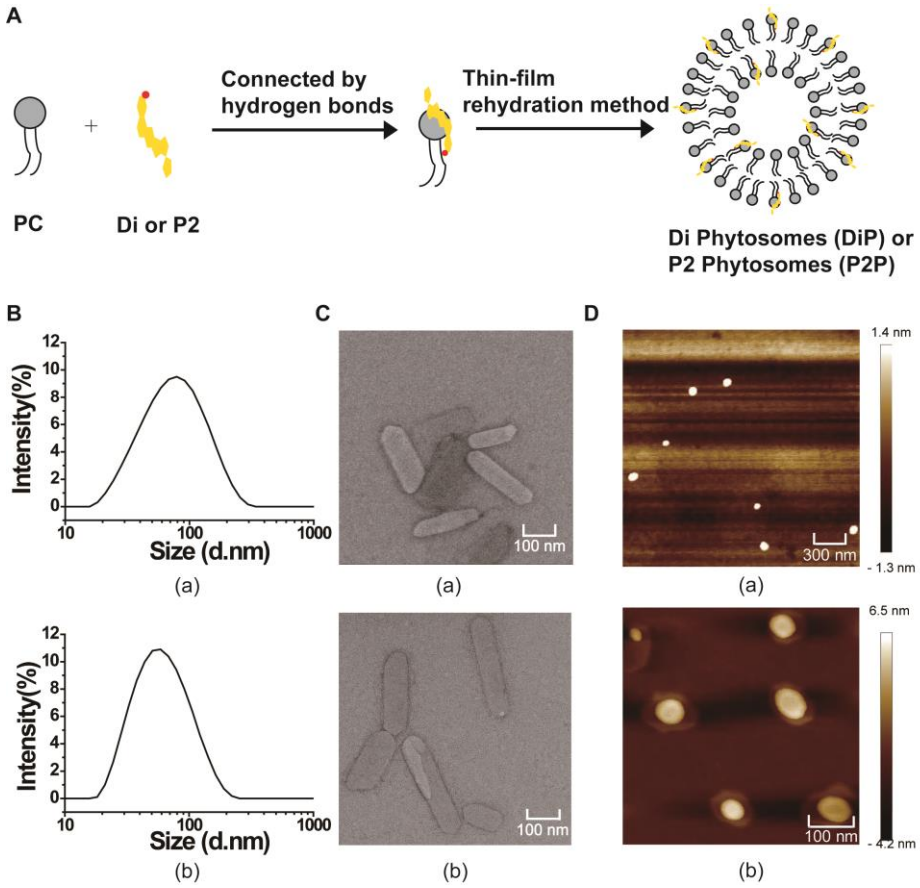

Figure 3 Preparation and characterization of Di phytosomes (DiP) and P2 phytosomes (P2P). (A) Schematic illustration of the preparation processes for DiP and P2P. (B) DLS measurements of DiP (a) and P2P (b). (C) TEM images of DiP (a) and P2P (b). (D) AFM images of DiP (a) and P2P (b).

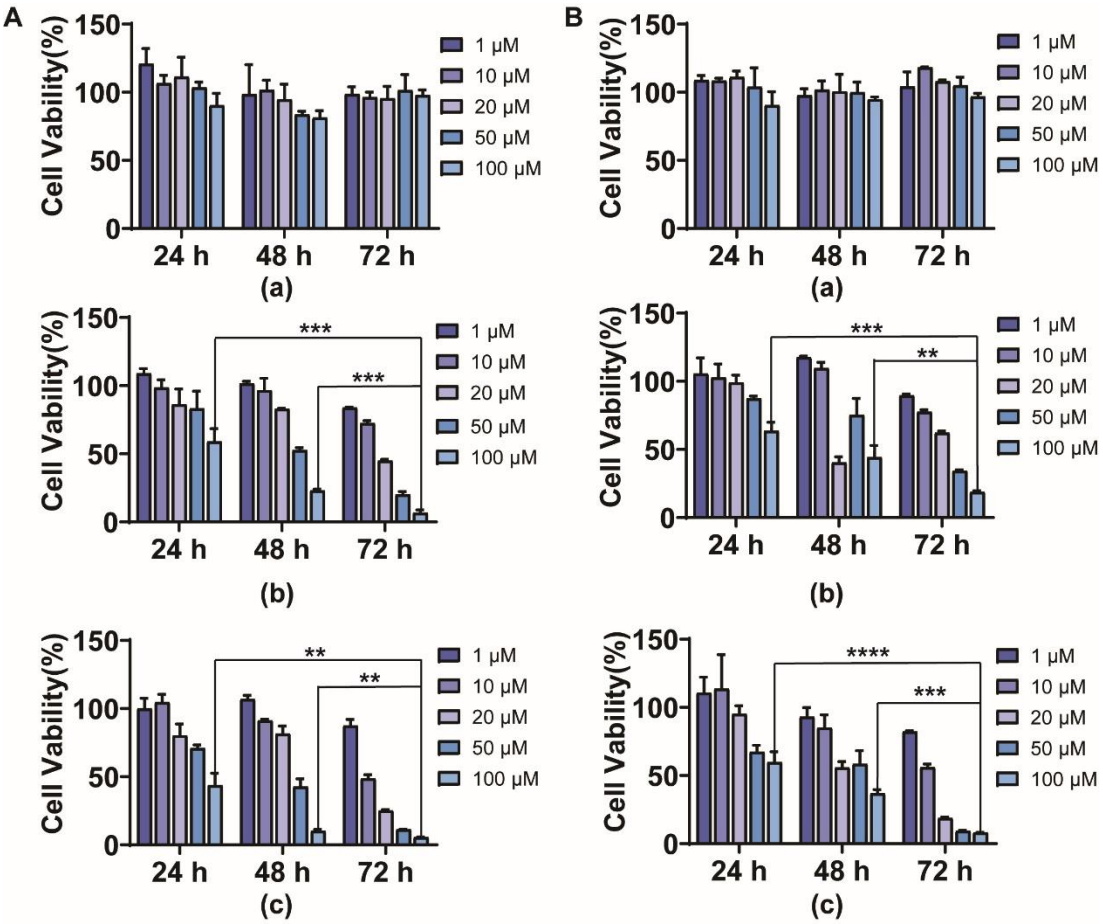

Figure 4 *In vitro* anti-proliferative activity of blank lipid nanoparticle (P), DiP, and P2P. (A) The cytotoxicity of different concentrations of P (a), DiP (b), and P2P (c) against A549 cells for 24, 48 and 72 h. (B) The cytotoxicity of different concentrations of P (a), DiP (b), and P2P (c) against PC9 cells for 24, 48 and 72 h. **p < 0.01 and ***p < 0.001 compared with 24-h or 48-h treatment group by Student's *t*-test.

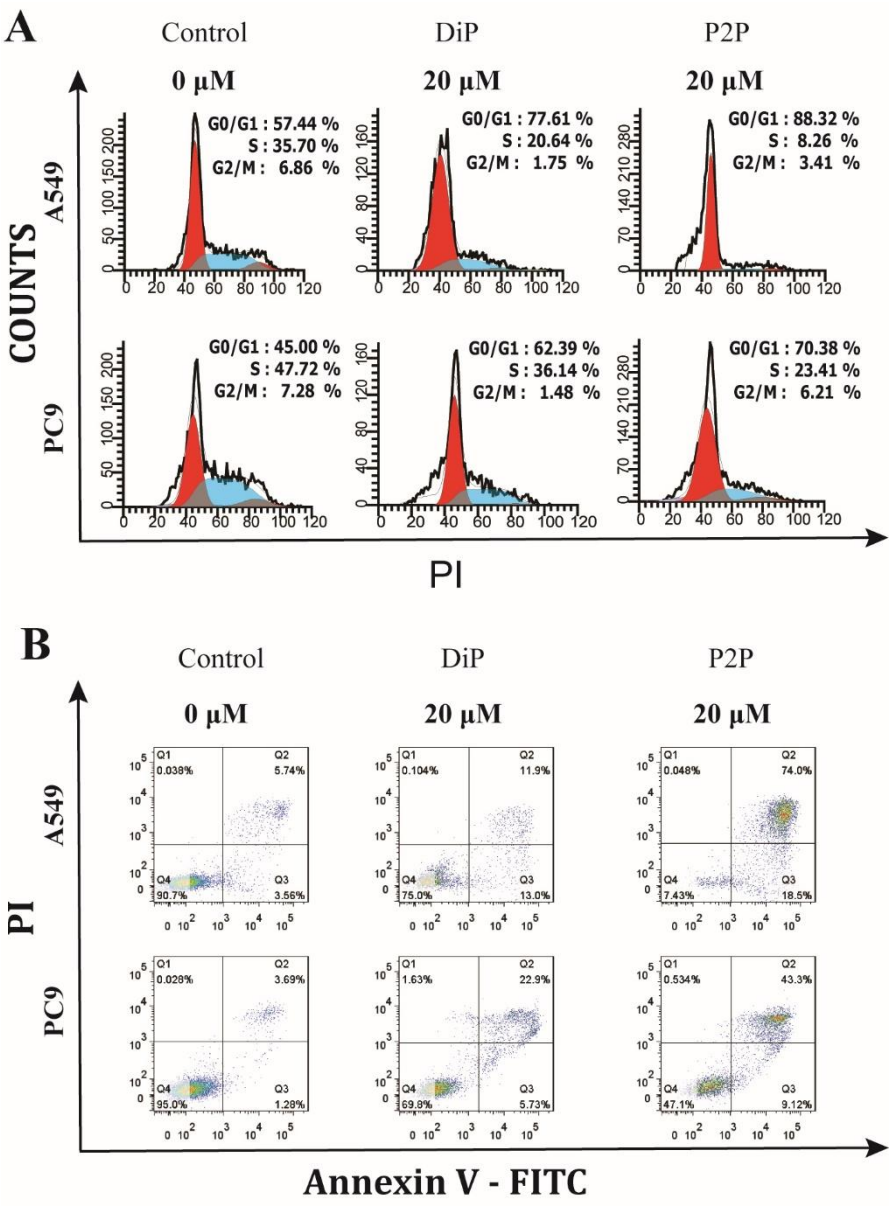

Figure 5 (A) Cell cycle analysis of A549 and PC9 cells after treated with DiP and P2P for 72 h. (B) Cell apoptosis analysis of A549 and PC9 cells after treated with DiP and P2P for 72 h.

Table 1 The IC_{50} values of diosgenin (Di), FZU-0021-194-P2 (P2) and their phytosomes against cancer cells by MTT assay.

NO	Samples	IC_{50}/μM			
		A549	**PC9**	**Hela**	**HepG2**
1	Di	55.0 (48 h)	85.8 (48 h)	~ 103.6 (48 h)	410.9 (48 h)
		39.9 (72 h)	51.7 (72 h)	-	-
2	P2	11.8 (48 h)	15.2 (48 h)	54.7 (48 h)	40.4(48 h)
		5.1 (72 h)	8.7 (72 h)	-	-
3	DiP[a]	18.0 (72 h)	29.1 (72 h)	-	-
4	P2P[b]	8.3 (72 h)	8.2 (72 h)	-	-

[a]DiP represents diosgenin phytosomes. [b]P2P represents FZU-0021-194-P2 phytosomes.

Table 2 Characterization of different phytosomes.

NO	Samples	Size/nm	PDI[d]	Zeta potential/mV
1	P[a]	139.8 ± 1.1	0.227 ± 0.014	−4.6 ± 0.2
2	DiP[b]	66.3 ± 0.3	0.268 ± 0.001	−6.4 ± 1.9
3	P2P[c]	53.6 ± 0.3	0.182 ± 0.008	−4.0 ± 0.7

[a]P represents blank lipid nanoparticles. [b]DiP represents diosgenin phytosomes. [c]P2P represents FZU-0021-194-P2 phytosomes. [d]PDI represents polydispersity index.